Automatica 121 (2020) 109192

Contents lists available at ScienceDirect

Automatica

journal homepage: www.elsevier.com/locate/automatica

Brief paper

On shortest Dubins path via a circular boundary☆

Bhargav Jha [a], Zheng Chen [b,*], Tal Shima [a]

[a] Department of Aerospace Engineering, Technion - Israel Institute of Technology, Haifa, 3200001, Israel
[b] School of Aeronautics and Astronautics, Zhejiang University, Hangzhou, 310027, China

ARTICLE INFO

Article history:
Received 14 February 2020
Received in revised form 28 May 2020
Accepted 9 July 2020
Available online 17 August 2020

Keywords:
Dubins path
Autonomous vehicles
Path planning
Motion control
Mobile robots
Optimal control

ABSTRACT

The paper characterizes the shortest bounded-curvature paths from an initial configuration (a location and a heading orientation), via the boundary of an intermediate circle, to a target configuration. Such paths are fundamentally required in motion planning of a Dubins vehicle that has to avoid entering certain forbidden regions and when addressing the Dubins Traveling Salesman Problem with Neighborhoods. By using Pontryagin's maximum principle and analyzing the necessary conditions for state inequality constraints, the geometric properties of the shortest bounded-curvature paths are established. These geometric properties not only allow restricting the shortest bounded-curvature path within a sufficient family of 26 candidates but also enable us to devise a completely analytic solution for finding the candidate path. As a consequence, the shortest bounded-curvature path can be computed in a constant time by checking the path lengths of these 26 candidates. Finally, numerical examples validate the developments in the paper and highlight its importance in addressing some Dubins Traveling Salesman Problems with Neighborhoods.

1. Introduction

In recent times, autonomous vehicles have become increasingly popular due to their wide applications such as surveillance, search and rescue, crop monitoring, and driver-less transportation, just to name a few. These vehicles operate in various environments such as land, air, marine, and even in space. In most real-world scenarios, motion planning of these vehicles from an initial point to a target point involves satisfying various constraints as discussed in LaValle (2006), Tsourdos, White, and Shanmugavel (2010) and references therein. Most of these constraints are vehicle-specific and the remaining arise from the complexity of the traversed environment. The vehicle-specific constraints take into account the constraints such as the minimum speed, the maximum maneuver capabilities (Manor, Ben-Asher, & Rimon, 2018), sensor configurations (Salaris, Cristofaro, Pallottino, & Bicchi, 2014; Tripathy & Sinha, 2017) *etc*. The presence of obstacles (Savkin & Hoy, 2013; Sunkara, Chakravarthy, & Ghose, 2019), the presence of other vehicles (Jha, Tsalik, Weiss, & Shima, 2019; Mylvaganam, Sassano, & Astolfi, 2017), adverse regions (Chen, 2020) where it is prohibited to enter, or the inherent shape of an environment (Matveev, Magerkin, & Savkin, 2020) are considered as environment specific constraints.

A popular problem in motion planning aims at finding the time optimal path between two configurations in $SE(2)$ (location and heading orientation), for a constant speed unidirectional non-holonomic vehicle subject to bounded-curvature constraints. This problem is an infinite dimensional optimization problem and was first proposed by Markov (1887) in the context of railway track design. In Dubins (1957) L. E Dubins proposed that the solution path for this problem belongs to a finite set of 6 types using geometrical analysis. Such vehicles are popularly denoted as Dubins vehicles and the aforementioned problem is called Dubins two-point problem. With the advent of Pontryagin's maximum principle (Pontryagin, 2018) and developments in optimal control theory (Gerdts, 2011; Girsanov, 2012; Ioffe & Tihomirov, 2009; Liberzon, 2011), an alternate proof appeared in Boissonnat, Cérézo, and Leblond (1994) and Johnson (1974). Extension of this problem for a bidirectional vehicle was solved in Reeds and Shepp (1990) and Sussmann and Tang (1991).

With the increasing emergence of practical applications of such vehicles, various classes of problems have stemmed out from the Dubins two-point problem. For example, the Dubins Traveling Salesman Problem (DTSP) aims at finding the shortest bounded-curvature path among a finite set of n points such that each point is visited exactly once. Achieving a global optimum for this problem involves combinatorial optimization to decide the

☆ This research was partially supported by the A. Pazy Research Foundation and National Natural Science Foundation of China under Grant No. 61903331. The material in this paper was partially presented at the 21st IFAC World Congress (IFAC 2020), July 12–17, 2020, Berlin, Germany. This paper was recommended for publication in revised form by Associate Editor Andrey V. Savkin under the direction of Editor Ian R. Petersen.

* Corresponding author.
E-mail addresses: jhabhargav@campus.technion.ac.il (B. Jha), z-chen@zju.edu.cn (Z. Chen), tal.shima@technion.ac.il (T. Shima).

https://doi.org/10.1016/j.automatica.2020.109192
0005-1098/

ordering of the target points and a continuous state optimization to decide an optimal heading at each target point. It was proved in Ny, Feron, and Frazzoli (2011) that such problems are NP-hard, thereby justifying the development of approximate and heuristic approaches to solve DTSP. In Isaiah and Shima (2015) and Ny et al. (2011), discretization based heuristic approaches were proposed to solve DTSP. Recently, using maximum principle, in Chen and Shima (2019) the authors considered DTSP with only three consecutive points and a complete analytical solution was provided.

Another class of problems that finds wide practical applications are DTSP with Neighborhoods (DTSPN). This variant differs from DTSP in a way that the target is a region instead of a point and each of these regions must be visited once. This problem is also NP-hard because as compared to DTSP, it has an additional complexity of finding the suitable point in the specified region. Therefore, heuristic and algorithmic based approaches instead of exact algorithms have been proposed for DTSPN as well. Obermeyer (2009) was the first to introduce this problem in context of surveillance mission by a fixed-wing aircraft and used genetic algorithm to solve it. Later on, two sampling based roadmap methods which transform a DTSPN to a generalized traveling salesman problem by Noon and Bean transformation (Noon & Bean, 1993) were proposed in Obermeyer, Oberlin, and Darbha (2012). Based on a similar approach, in Isaacs and Hespanha (2013) and Isaacs, Klein, and Hespanha (2011) a more general version of Noon and Bean transformation was used. This approach resulted in a shorter path compared to Obermeyer et al. (2012) in case of overlapping target regions. In Guimaraes Macharet, Alves Neto, Fiuza da Camara Neto, and Montenegro Campos (2012) an evolutionary algorithm was used to solve DTSPN.

The aforementioned approaches for DTSPN are either discretization based approaches in which the optimization errors depend on the resolution of the discretization, or they are evolutionary approaches which result in accurate solutions but have high computational cost as recently reported in Váňa and Faigl (2015). In Váňa and Faigl (2015), based on the development in Goaoc, Kim, and Lazard (2013), an alternate approach is proposed which promises accurate solutions at par with evolutionary approaches and has low computational demands. Under the assumption that the target regions are separated at least by four times the minimum curvature of the path, the authors propose that knowing some geometrical properties of the optimal path can bring down the computational time by at least an order of magnitude. With the same assumption about the separation of target regions, Chen, Sun, Shao, and Zhao (2020) present a formulation using coordinate descent optimization (Wright, 2015) method for DTSPN. The core idea of the descent algorithm is to decompose DTSPN into a series of subproblems, each of which is of finding the shortest Dubins path from a fixed configuration, via an intermediate circle, to another fixed configuration. Both the approaches in Chen et al. (2020) and Váňa and Faigl (2015) rely on solving the simple subproblem. Even though the computational time to solve the subproblem largely determines the efficiency of the descent algorithm, a thorough analytical solution of the subproblem has not been presented in Chen et al. (2020) and Váňa and Faigl (2015).

Besides being important in solving DTSPN, the solution of the mentioned subproblem is also widely required in other real-world applications. Some of the key applications include surveillance and imaging of restricted regions by a fixed-wing unmanned aerial vehicle (UAV), and path planning for a Dubins car to avoid circular obstacle which interferes with the shortest path between two configurations (Savkin & Hoy, 2013). Yet, the authors are not aware of any literature on characterization of the solution of the subproblem. For this reason, this paper aims

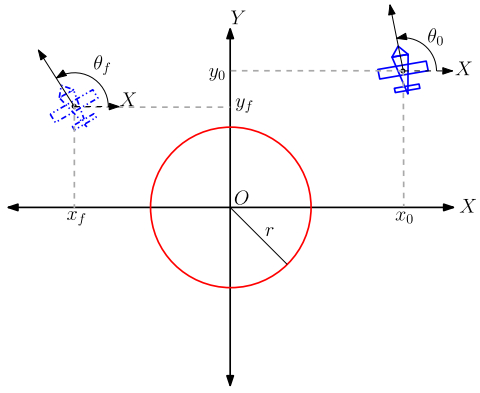

Fig. 1. Engagement Geometry.

at characterizing the shortest bounded-curvature path from an initial configuration, via the boundary of an intermediate circle, to a target configuration. Some fundamental geometric properties of the shortest path are established which lead to the reduction in the number of candidate solutions from an infinite number of possible paths to a finite set of only 26 paths. It is shown that each candidate is related to a zero of an equation in terms of the known problem parameters, thus providing a complete analytical solution. As a result, given any problem parameters, the shortest bounded-curvature path can be found efficiently. Moreover, the developments of this paper do not consider any assumption on the distances between initial and final configurations from the intermediate circle. This facilitates the application of the descent method for DTSPNs (Chen et al., 2020; Váňa & Faigl, 2015) even in the scenarios where the assumption that the target regions are separated at least by four times the minimum curvature is relaxed. This is demonstrated by the numerical simulations in Section 6.

At a preliminary stage, some results of the paper appear in Jha, Chen, and Shima (2020). In this work we have expanded on these results by proposing more geometrical properties of the optimal path and establishing analytical solutions for all the categories of the optimal path.

2. Problem formulation

Consider a circular region of radius $r \in \mathbb{R}^+$ with its center at the origin of an inertial coordinate system OXY, as represented in Fig. 1. For notational simplicity, hereafter we denote this circle by $\mathcal{C}$, *i.e.*,

$$\mathcal{C} = \{(x, y) \in \mathbb{R}^2 | x^2 + y^2 = r^2\}$$

In the frame OXY, the state $\mathbf{x} = [x, y, \theta]^\top$, also called configuration, represents the position $(x, y) \in \mathbb{R}^2$ and the orientation angle $\theta \in \mathbb{S}^1$ of a Dubins vehicle whose minimum turn radius is $\rho \in \mathbb{R}^+$. The kinematics of this vehicle is expressed as

$$\frac{\mathrm{d}\mathbf{x}}{\mathrm{d}t} = f(\mathbf{x}, u), \quad u \in [-1, 1] \tag{1}$$

where $f(\mathbf{x}, u)$ is given as,

$$f(\mathbf{x}, u) = \begin{bmatrix} \cos\theta & \sin\theta & \frac{u}{\rho} \end{bmatrix}^\top$$

Here, $u \in [-1, 1]$ is the control input and t denotes time. The paper aims to find the shortest path for Dubins vehicle from an initial configuration $\mathbf{x_0} = [x_0,\ y_0,\ \theta_0]^\top$ at time $t_0 \in \mathbb{R}^+$ to a given final configuration $\mathbf{x_f} = \begin{bmatrix} x_f,\ y_f,\ \theta_f \end{bmatrix}^\top$ via the boundary of the circle $\mathcal{C}$. Denote by $t_f > t_0$ the time at which the Dubins vehicle

reaches the final configuration, and by $t_1 \in (t_0, t_f)$ and $t_2 \in [t_1, t_f)$ the times of reaching and exiting the circle $\mathcal{C}$, respectively.

In order to avoid entering inside the circle $\mathcal{C}$, the following state inequality constraint must be satisfied,

$$S(\mathbf{x}, t) = \frac{1}{2}\left(x^2 + y^2 - r^2\right) \geq 0 \tag{2}$$

At the final time, the following terminal constraint must also be satisfied,

$$\mathbf{M}(t_f) \triangleq \begin{bmatrix} x(t_f) - x_f & y(t_f) - y_f & \theta(t_f) - \theta_f \end{bmatrix}^\top = [\mathbf{0}]_{3\times 1}$$

To find the shortest path, the cost function to be minimized is defined as,

$$J = \int_{t_0}^{t_f} 1 \, \mathrm{d}t$$

After formulating the problem, in the next section we will consider the necessary conditions for the optimal control problem with state inequality constraints.

3. Necessary conditions for optimal path generation

Constraint in Eq. (2) is a pure state inequality constraint. Such constraints can be equivalently handled by direct or indirect adjoining methods as discussed in Hartl, Sethi, and Vickson (1995). Here, we will use indirect adjoining method for which the first order necessary conditions were proposed in Bryson, Denham, and Dreyfus (1963) and additional necessary conditions were proposed in Kreindler (1982).

During the time interval when the path of the Dubins vehicle is on the circle $\mathcal{C}$, we have

$$S(\mathbf{x}, t) = 0, \quad t \in [t_1, t_2]$$

In a non-zero interval $[t_1, t_2]$, the higher order derivatives of $S(\mathbf{x}, t)$ with respect to time must also identically vanish. In order to make the constraint an explicit function of control u, we obtain the higher derivatives until u reappears:

$$\dot{S} \triangleq \frac{\mathrm{d}S}{\mathrm{d}t} = x\cos\theta + y\sin\theta = 0 \tag{3a}$$

$$\ddot{S} \triangleq \frac{\mathrm{d}^2 S}{\mathrm{d}t^2} = 1 + (y\cos\theta - x\sin\theta)\frac{u}{\rho} = 0 \tag{3b}$$

From Eq. (3b), $\ddot{S} = 0$ gives the control on the circular boundary of $\mathcal{C}$ as

$$u = -\frac{\rho}{(y\cos\theta - x\sin\theta)} \tag{4}$$

Remark 1. On the constraint boundary ($S = 0$, $\dot{S} = 0$), the heading direction of the Dubins vehicle is tangent to the circle. Therefore, we have $|(y\cos\theta - x\sin\theta)| = r$ on the constraint boundary, where $|\cdot|$ denotes the absolute value. It should be noted that the control in Eq. (4) is only realizable if $r \geq \rho$.

In addition to the above conditions on the constrained boundary, the following interior point conditions must also hold at t_1,

$$N(\mathbf{x_1}(t_1), t_1) \triangleq \begin{bmatrix} \frac{1}{2}[x(t_1)^2 + y(t_1)^2 - r^2] \\ x(t_1)\cos\theta(t_1) + y(t_1)\sin\theta(t_1) \end{bmatrix} = 0 \tag{5}$$

Denote by $\boldsymbol{p} = [p_x, p_y, p_\theta]^\top$ the costate of $\boldsymbol{x}$. Along with the above constraint conditions, the Hamiltonian $H(\mathbf{p}, \mathbf{x}, u)$ for the problem is defined as,

$$H(\mathbf{p}, \mathbf{x}, u) = p_0 + p_x\cos\theta + p_y\sin\theta + p_\theta\frac{u}{\rho} + \lambda\ddot{S} \tag{6}$$

where λ is a scalar given by

$$\lambda(t) = \begin{cases} > 0, & \text{if } S(x,t) = 0, \\ = 0, & \text{if } S(x,t) > 0 \end{cases} \tag{7}$$

As abnormal solutions, for which $p_0 = 0$, are ruled out in Sussmann and Tang (1991), we have $p_0 < 0$. Therefore, along the optimal trajectory the rest of the costates can be normalized so that $p_0 = -1$. Using variational approach, it was proposed in Bryson et al. (1963) that the following first order necessary conditions must hold,

$$\mathbf{p}(t_1^-) = \mathbf{p}(t_1^+) + \frac{\partial N(\mathbf{x}, t)}{\partial \mathbf{x}}^\top \boldsymbol{\mu}\Big|_{t=t_1} \tag{8a}$$

$$H(\mathbf{p}^*, \mathbf{x}^*, u^*)\big|_{t_1^-} = H(\mathbf{p}^*, \mathbf{x}^*, u^*)\big|_{t_1^+} \tag{8b}$$

$$\mathbf{p}(t_2^-) = \mathbf{p}(t_2^+) \tag{8c}$$

$$H(\mathbf{p}^*, \mathbf{x}^*, u^*)\big|_{t_2^-} = H(\mathbf{p}^*, \mathbf{x}^*, u^*)\big|_{t_2^+} \tag{8d}$$

where $\boldsymbol{\mu} = [\mu_1 \ \mu_2]^\top$ is a two-dimensional vector, and t_i^- and t_i^+ denote the time just before and after t_i ($i = 1, 2$), respectively. The conditions involving the jump in the costates (Eqs. (8a) and (8c)) translate to,

$$p_x(t_1^-) = p_x(t_1^+) + \mu_1 x(t_1) + \mu_2\cos\theta(t_1) \tag{9a}$$

$$p_y(t_1^-) = p_y(t_1^+) + \mu_1 y(t_1) + \mu_2\sin\theta(t_1) \tag{9b}$$

$$p_\theta(t_1^-) = p_\theta(t_1^+) + \mu_2\left(y(t_1)\cos\theta(t_1) - x(t_1)\sin\theta(t_1)\right) \tag{9c}$$

$$p_x(t_2^-) = p_x(t_2^+) \tag{9d}$$

$$p_y(t_2^-) = p_y(t_2^+) \tag{9e}$$

$$p_\theta(t_2^-) = p_\theta(t_2^+) \tag{9f}$$

Additional necessary conditions proposed in Kreindler (1982) are as follows,

$$\mu_1 - \dot{\lambda}\left(t_1^+\right) \geq 0 \tag{10a}$$

$$\mu_2 + \lambda\left(t_1^+\right) = 0 \tag{10b}$$

$$-\dot{\lambda}\left(t_2^-\right) \geq 0 \tag{10c}$$

$$\lambda\left(t_2^-\right) \geq 0 \tag{10d}$$

$$\ddot{\lambda}(t) \geq 0 \qquad t \in [t_1, t_2] \tag{10e}$$

According to transversality conditions, the costate should be orthogonal to the tangent space of the terminal manifold. Therefore the following equation is satisfied,

$$\mathbf{p}(t_f) = \boldsymbol{\beta}^\top \frac{\partial \mathbf{M}}{\partial \mathbf{x_f}}$$

where $\boldsymbol{\beta} \in \mathbb{R}^3$ is a constant vector. The costates should satisfy the following Euler–Lagrange equations,

$$\dot{\mathbf{p}} = \begin{cases} -\left[\frac{\partial f}{\partial \mathbf{x}}\right]^\top \mathbf{p}, & S > 0 \\ -\left[\frac{\partial f}{\partial \mathbf{x}} - \frac{\partial f}{\partial u}\left(\frac{\partial \ddot{S}}{\partial u}\right)^{-1}\frac{\partial \ddot{S}}{\partial \mathbf{x}}\right]^\top \mathbf{p}, & S = 0 \end{cases}$$

This gives us the following equations,

$$\dot{p}_x = \begin{cases} 0, & S > 0 \\ p_\theta\sin\theta, & S = 0 \end{cases} \tag{11a}$$

$$\dot{p}_y = \begin{cases} 0, & S > 0 \\ -p_\theta\cos\theta, & S = 0 \end{cases} \tag{11b}$$

$$\dot{p}_\theta = \begin{cases} p_x\sin\theta - p_y\cos\theta, & S > 0 \\ \frac{-p_x(t)\sin\theta + p_y(t)\cos\theta}{r^2}, & S = 0 \end{cases} \tag{11c}$$

From Eqs. (11), p_θ is expressed as,

$$p_\theta(t) = \begin{cases} p_x(t_1^-)y - p_y(t_1^-)x + c_1, & t \in [t_0, t_1^-) \\ p_x(t_2^+)y - p_y(t_2^+)x + c_2, & t \in (t_2^+, t_f] \end{cases} \tag{12}$$

where $c_1, c_2 \in \mathbb{R}$ are constants of integration. Eliminating μ_1 and μ_2 from Eqs. (9a)–(9c) yields,

$$p_x(t_1^-)y(t_1) - p_y(t_1^-)x(t_1) = p_x(t_1^+)y(t_1) - p_y(t_1^+)x(t_1) + \mu_2(y(t_1)\cos\theta(t_1) - x(t_1)\sin\theta(t_1))$$

Combining this equation with Eq. (12) leads to

$$p_\theta(t_1^+) = c_1 + p_x(t_1^+)y(t_1) - p_y(t_1^+)x(t_1) \tag{13}$$

Now, according to maximum principle (Pontryagin, 2018), the optimal control u^* along the unconstrained path ($S \geq 0$) is given as,

$$u^* = \arg\max_{u\in[-1,1]} H(\mathbf{p}, \mathbf{x}, u)$$

indicating

$$u^* = \begin{cases} -1 & p_\theta < 0 \\ 0 & p_\theta = 0 \\ 1 & p_\theta > 0 \end{cases} \tag{14}$$

The singular control for $p_\theta(\cdot) \equiv 0$ is obtained from Eq. (12), which suggests that for any non-zero interval $[t_a, t_b] \subset [t_0, t_f]$ if $p_\theta(\cdot) \equiv 0$, then the path in $X-Y$ plane is a straight line, implying $u(t) = 0,\ t \in [t_a, t_b]$. On the constrained arc, the control is given by Eq. (4). This shows that the time optimal path can only be a concatenation of three categories of segments namely, straight line segment (S), circular arc (C) with radius ρ which can either be a right turn (R) or a left turn (L), and circular arc (O) with radius r centered at the origin. The segment (O) can either be in clockwise or counter-clockwise direction.

Assumption 1. It should be noted that for some problem parameters there may not exist any admissible solution. The characterization of the path in the next section will be done based on an assumption that an optimal path exists for the optimal control problem.

4. Characterization of the optimal path

In this section, we will characterize the properties of the shortest bounded curvature paths. Note that there are only two distinct cases for the tangency between the optimal path and the intermediate circle $\mathcal{C}$: (1) the optimal path has only one point tangent to $\mathcal{C}$ at time t_1 and (2) the optimal path overlaps the boundary of the circle $\mathcal{C}$ on a nonzero interval $[t_1\ t_2]$ where $t_1 \neq t_2$. In the following two subsections, we will characterize the optimal path of the two cases independently.

Remark 2. If $r > \rho$, it is apparent that the optimal path has only one point tangent to $\mathcal{C}$ if the shortest Dubins path from initial to final configuration does not intersect the intermediate circle $\mathcal{C}$. If it does, then a segment O will appear in the optimal path.

4.1. Optimal path with only one point tangent to $\mathcal{C}$

Lemma 4.1. *If the optimal path has only one point tangent to the intermediate circle $\mathcal{C}$ at time t_1, then $p_\theta(t)$ is continuous at t_1.*

Proof. Due to tangency at single point we have $S(\mathbf{x}, t_1^+) > 0$ and $\lambda(t_1^+) = 0$ from Eq. (7). Therefore from Eq. (10b) $\mu_2 = 0$. Hence we obtain $p_\theta(t_1^-) = p_\theta(t_1^+)$, thereby completing the proof. □

Remark 3. An alternate proof for Lemma 4.1 using only necessary conditions of Bryson et al. (1963) appears in Jha et al. (2020). The work in Bryson et al. (1963) under-specifies the conditions at the junction points as stated in Jacobson, Lele, and Speyer (1971). Conditions in Kreindler (1982) close this gap and facilitate simpler proof in our case.

Corollary 1. *The segment of the optimal path before and after the tangent point can only be one of the types from the set $\{R|R,\ L|L,\ S|S\}$, where '|' represent the concatenation of the segments.*

Proof. The proof follows immediately from Lemma 4.1 □

It should be noted that the solutions both before and after t_1 are of type *CSC* or *CCC* or their substrings due to Dubins (1957). Therefore, by Bellman's optimality principle (Bellman, 1966), the optimal path can belong to a type of *CSC*|*CSC*, *CSC*|*CCC*, *CCC*|*CSC*, or *CCC*|*CCC*. Considering that a circular arc C can be either an R or an L, the total types are up to 36. But using Corollary 1, the optimal path candidates can be reduced to one of the 18 types such as *CSCSC*, *CSCCC*, *CCCSC*, and *CCCCC*.

Theorem 4.2. *Let $\mathcal{L}_1$ and $\mathcal{L}_2$ denote the straight lines joining all the points with $p_\theta = 0$ before and after the tangent point, respectively. Then the tangent point of the optimal path and $\mathcal{C}$, the point of intersection of $\mathcal{L}_1$ and $\mathcal{L}_2$ and the origin are collinear.*

Proof. According to Eqs. (12) and (13), we have $c_1 = c_2$. Then, the expression of p_θ is given by

$$p_\theta(t) = \begin{cases} p_x(t_1^-)y(t) - p_y(t_1^-)x(t) + c_1, & t \in [t_0, t_1) \\ p_x(t_1^+)y(t) - p_y(t_1^+)x(t) + c_1, & t \in (t_1, t_f] \end{cases} \tag{15}$$

The equations of lines $\mathcal{L}_1$ and $\mathcal{L}_2$ will be given by $p_x(t_1^-)y(t) - p_y(t_1^-)x(t) + c_1 = 0$ and $p_x(t_1^+)y(t) - p_y(t_1^+)x(t) + c_1 = 0$. Solving these two equations simultaneously gives us the point of intersection (say (x_c, y_c)) as,

$$x_c = c_1 \frac{p_x(t_1^-) - p_x(t_1^+)}{p_y(t_1^+)p_x(t_1^-) - p_x(t_1^+)p_y(t_1^-)}$$

$$y_c = c_1 \frac{p_y(t_1^-) - p_y(t_1^+)}{p_y(t_1^+)p_x(t_1^-) - p_x(t_1^+)p_y(t_1^-)}$$

Using the necessary conditions from Eqs. (9a)–(9b) and the fact that $\mu_2 = 0$ from Corollary 1 and Lemma 4.1, we have the following relation,

$$\frac{x_c}{y_c} = \frac{x(t_1)}{y(t_1)}$$

This shows that points $(x(t_1), y(t_1))$, (x_c, y_c), $(0, 0)$ are colinear, thereby completing the proof. □

Corollary 2. *Assume that the optimal path before t_1 is of type $C_1S_2C_3$ and that the path after t_1 is of type $C_4S_5C_6$, then the arc lengths of C_3 and C_4 are equal to each other.*

Proof. From Eqs. (14) and (15), we have that $p_x(t_1^-)y - p_y(t_1^-)x + c_1 = 0$ and $p_x(t_1^+)y - p_y(t_1^+)x + c_1 = 0$ along S_2 and S_5, respectively. The perpendicular distances from the center of C_3 and C_4 to the two straight lines $p_x(t_1^-)y - p_y(t_1^-)x + c_1 = 0$ and $p_x(t_1^+)y - p_y(t_1^+)x + c_1 = 0$ are equal to each other, because S_2 and S_5 are tangent to C_3 and C_4, respectively. Then, using results from Theorem 4.2 it can be geometrically shown that the perpendicular distances from the tangent point $(x(t_1), y(t_1))$ to the two straight lines $p_x(t_1^-)y - p_y(t_1^-)x + c_1 = 0$ and $p_x(t_1^+)y - p_y(t_1^+)x + c_1 = 0$ are equal to each other, as illustrated in Fig. 2. Therefore, we have that the arc lengths of C_3 and C_4 are identical, completing the proof. □

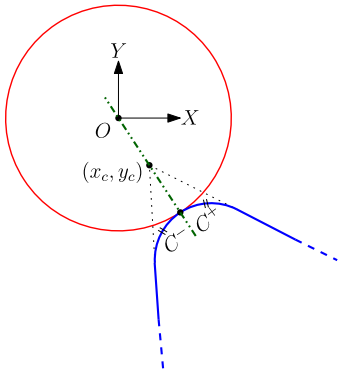

Fig. 2. Geometrical properties of *CSCSC* optimal path.

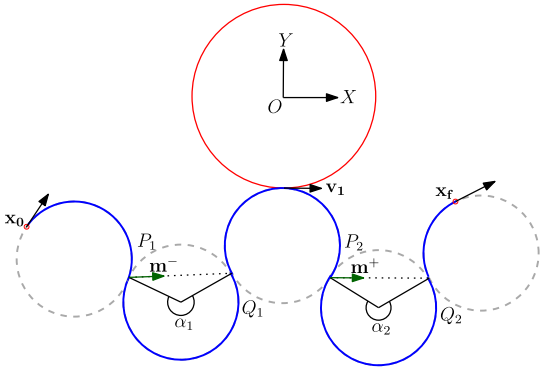

Fig. 3. Geometry of a *RLRLR* path.

Theorem 4.3. *If the optimal path is $C_1X_1C_2X_2C_3$, $X_{i=\{1,2\}} \in \{C, S\}$ such that none of the subarcs vanishes, then*

$$\left\langle \cos\frac{\alpha_2}{2}\mathbf{m}^- - \cos\frac{\alpha_1}{2}\mathbf{m}^+, \mathbf{v_t} \right\rangle = 0$$

where $\langle \mathbf{i}, \mathbf{j} \rangle$ denotes the inner product of $\mathbf{i}$ and $\mathbf{j}$, $\mathbf{m}^-$ and $\mathbf{m}^+$ are the unit vectors in the direction of line segments joining all the points with $p_\theta(t) = 0$ before and after the tangent point, respectively, and $\mathbf{v_t}$ is the velocity vector at the tangent point. If $X_{i=\{1,2\}} = C$, then $\alpha_{i=\{1,2\}}$ is the radian of the circular arc and if $X_{i=\{1,2\}} = S$ then $\alpha_{i=\{1,2\}} = 0$.

Proof. Without loss of generality, we consider the optimal path of type *RLRLR* as shown in Fig. 3. (Note that this figure is intended to represent only the geometry of *RLRLR* path and not necessarily an optimal path between the configurations shown there. Other figures shown before Section 6 are also drawn in the same spirit.) For other optimal path types, the proof is along the same lines. Express $p_x(t_1^-) = \lambda^- \cos(\sigma^-)$ and $p_y(t_1^-) = \lambda^- \sin(\sigma^-)$ for some constant $\lambda^- \in \mathbb{R}^+$ and $\sigma^- \in \mathbb{R}$. Similarly, we express $p_x(t_1^+) = \lambda^+ \cos(\sigma^+)$ and $p_y(t_1^+) = \lambda^+ \sin(\sigma^+)$ for some constant $\lambda^+ \in \mathbb{R}^+$ and $\sigma^+ \in \mathbb{R}$. P_i and Q_i, $i \in 1, 2$ are the end points of segment X_i as shown in Fig. 3. By maximum principle, $H(\mathbf{p}^*, \mathbf{x}^*, u^*) = 0$. Hence, considering the heading at P_1 as β_1, we have at P_1 and Q_1,

$$\begin{aligned}&\lambda^- \cos(\sigma^-)\cos(\beta_1) + \lambda^- \sin(\sigma^-)\sin(\beta_1) - 1\\ =&\lambda^- \cos(\sigma^-)\cos(\beta_1+\alpha_1) + \lambda^- \sin(\sigma^-)\sin(\beta_1+\alpha_1) - 1\\ =&0\end{aligned}$$

Solving the first equality we obtain,

$$\sin(\frac{\alpha_1}{2})\sin(\sigma^- - \beta_1 - \frac{\alpha_1}{2}) = 0$$

Since $\alpha_1 \in (\pi, 2\pi)$ according to Lemma 3 of Bui, Boissonnat, Soueres, and Laumond (1994), it follows $\sin(\alpha_1/2) \neq 0$, indicating $\sigma^- = \beta_1 + \frac{\alpha_1}{2} + k\pi$, $k \in \mathbb{Z}$. Substituting it into the second equality, we have $\lambda^- = \frac{1}{\cos(\alpha_1)}$. Similarly, considering the heading at P_2 as β_2, we have at P_2 and Q_2,

$$\begin{aligned}&\lambda^+ \cos(\sigma^+)\cos(\beta_2) + \lambda^+ \sin(\sigma^+)\sin(\beta_2) - 1\\ =&\lambda^+ \cos(\sigma^+)\cos(\beta_2+\alpha_2) + \lambda^+ \sin(\sigma^+)\sin(\beta_2+\alpha_2) - 1\\ =&0\end{aligned}$$

Solving it similarly as before, we obtain $\sigma^+ = \beta_2 + \frac{\alpha_2}{2} + k\pi$, $k \in \mathbb{Z}$ and $\lambda^+ = \frac{1}{\cos(\alpha_2)}$.

Let the heading angle at the tangent point be θ_1, then the tangent point is $[r\sin(\theta_1), -r\cos(\theta_1)]$. By necessary conditions in Eqs. (9a)–(9b) and the fact that $\mu_2 = 0$ from Corollary 1 and Lemma 4.1, we have

$$\frac{\lambda^- \cos(\sigma^-) - \lambda^+ \cos(\sigma^+)}{\lambda^- \sin(\sigma^-) - \lambda^+ \sin(\sigma^+)} = -\frac{\sin(\theta_1)}{\cos(\theta_1)}$$

By rearranging the terms we obtain,

$$\left\langle \lambda^+ \begin{bmatrix}\cos\sigma^-\\ \sin\sigma^-\end{bmatrix} - \lambda^- \begin{bmatrix}\cos\sigma^+\\ \sin\sigma^+\end{bmatrix}, \begin{bmatrix}\cos\theta_1\\ \sin\theta_1\end{bmatrix} \right\rangle = 0 \tag{16}$$

Before the tangent point, the segment joining all points with $p_\theta(t) = 0$ is given by $\lambda^- \cos\sigma^- y - \lambda^+ \sin\sigma^+ x + c_1 = 0$ and hence the unit vector parallel to this line is $[\cos\sigma^- \quad \sin\sigma^-]^\top$. Similarly, for the points $p_\theta(t) = 0$ after the tangent point, we have the unit vector as $[\cos\sigma^+ \quad \sin\sigma^+]^\top$. Therefore, Eq. (16) can be rewritten as,

$$\left\langle \cos\frac{\alpha_2}{2}\mathbf{m}^- - \cos\frac{\alpha_1}{2}\mathbf{m}^+, \mathbf{v_t} \right\rangle = 0 \tag{17}$$

which completes the proof. □

4.2. Optimal path with a nonzero interval overlapping $\mathcal{C}$

Now, we will characterize the properties of the optimal path when a segment of the path overlaps the boundary of the intermediate circle $\mathcal{C}$. As mentioned before, we denote such segments as O. It should be noted from Remark 1 that such segments occur only if $\rho < r$. Let us denote the time of entry to the circular boundary as t_1 and time of exit as t_2.

Lemma 4.4. *If $\rho < r$, then the segment O in an optimal path cannot be preceded or succeeded by a circular arc C.*

Proof. Let us assume that the segment O is preceded by a segment C. Then, we have $u\left(t_1^-\right) = \pm 1$ implying $p_\theta\left(t_1^-\right) \neq 0$ and from Eq. (4), $u\left(t_1^+\right) = -\frac{\rho}{(y(t_1)\cos\theta(t_1) - x(t_1)\sin\theta(t_1))}$. Using the continuity of the Hamiltonian at the entry point from Eq. (8b) we have,

$$\begin{aligned}&p_0 + p_x\left(t_1^-\right)\cos\theta\left(t_1^-\right) + p_y\left(t_1^-\right)\sin\theta\left(t_1^-\right) + p_\theta\left(t_1^-\right)\frac{u(t_1^-)}{\rho} =\\ &p_0 + p_x\left(t_1^+\right)\cos\theta\left(t_1^+\right) + p_y\left(t_1^+\right)\sin\theta\left(t_1^+\right) + p_\theta\left(t_1^+\right)\frac{u(t_1^+)}{\rho}\end{aligned} \tag{18}$$

By rearranging Eq. (18) and using the necessary conditions from Eqs. (9a)–(9c) $p_\theta\left(t_1^-\right)$ can be expressed as,

$$p_\theta\left(t_1^-\right) = -\mu_2 \frac{\left(\rho + (y(t_1)\cos\theta(t_1) - x(t_1)\sin\theta(t_1))\, u\left(t_1^+\right)\right)}{u\left(t_1^-\right) - u\left(t_1^+\right)}$$

Now substituting the value of $u\left(t_1^+\right)$ and $u\left(t_1^-\right)$ in the above equation, we obtain $p_\theta\left(t_1^-\right) = 0$. This is a contradiction. Hence, a segment O cannot be preceded by a segment C.

If a path from initial to final configuration is optimal, then the path from final to initial condition with a backward speed

is also optimal. Therefore, the necessary conditions for entry and exit points in Eqs. (8) can be interchanged and it can be shown that a segment O cannot be succeeded by a segment C. Hence, completing the proof. □

The result of Lemma 4.4 concurs with the result of Theorem 3.1 in Savkin and Hoy (2013), where geometric arguments are used to proof similar result for any smooth boundary of an obstacle under some assumption of minimum distance of initial and final point from the obstacle.

Corollary 3. *If $\rho < r$ and the optimal path contains an O-segment, then the optimal path can only be of type CSOSC or its substring.*

Proof. The proof follows immediately from Lemma 4.4 and Dubins (1957). □

This suggests that the total number of optimal path types is 26. This includes the 18 types in case of the optimal path having only tangent point and additional 8 types when the optimal path has non zero interval overlapping $\mathcal{C}$.

Theorem 4.5. *If the optimal path is of type CS_1OS_2C such that none of the subarcs vanishes and θ_i, $i \in \{1, 2\}$ denote the angle formed by segment S_i from the positive direction of $X-$axis, then the equations of the lines are given as,*

$$S_1: \ \cos\theta_1 y - \sin\theta_1 x + \delta r = 0$$
$$S_2: \ \cos\theta_2 y - \sin\theta_2 x + \delta r = 0$$

where $\delta = 1$ if O is in anticlockwise direction and $\delta = -1$ if O is in clockwise direction.

Proof. Let us assume the case when segment O is in clockwise direction. As done previously, let $p_x(t_1^-) = \lambda^- \cos(\sigma^-)$ and $p_y(t_1^-) = \lambda^- \sin(\sigma^-)$ for some constant $\lambda^- \in \mathbb{R}^+$ and $\sigma^- \in \mathbb{R}$ and $p_x(t_1^+) = \lambda^+ \cos(\sigma^+)$ and $p_y(t_1^+) = \lambda^+ \sin(\sigma^+)$ for some constant $\lambda^+ \in \mathbb{R}^+$ and $\sigma^+ \in \mathbb{R}$. As $p_\theta(t) = 0$ along the segments S_1 and S_2, then from Eq. (12), their equations are given as,

$$S_1: \ \lambda^- \cos(\sigma^-) y - \lambda^- \sin(\sigma^-) x + c_1 = 0$$
$$S_2: \ \lambda^+ \cos(\sigma^+) y - \lambda^+ \sin(\sigma^+) x + c_2 = 0$$

The slope of S_i is given as $\tan(\theta_i)$, therefore we have $\sigma^- = \theta_1 + n\pi$ for $n \in \mathbb{Z}$ and $\sigma^+ = \theta_2 + n\pi$ for $n \in \mathbb{Z}$. Due to Pontryagin (2018), along the optimal path $H(\mathbf{p}^*, \mathbf{x}^*, u^*) = 0$. Therefore, it follows that along the segment S_1,

$$\lambda^- \cos(\theta_1)\cos(\theta_1) + \lambda^- \sin(\theta_1)\sin(\theta_1) - 1 = 0$$

and along S_2 we have,

$$\lambda^+ \cos(\theta_2)\cos(\theta_2) + \lambda^+ \sin(\theta_2)\sin(\theta_2) - 1 = 0$$

From the above two equations, $\lambda^- = \lambda^+ = 1$. Now, as S_1 and S_2 are tangent to circle $\mathcal{C}$, they must pass through point $[-r\sin(\theta_1) \quad r\cos(\theta_1)]$ and $[-r\sin(\theta_2) \quad r\cos(\theta_2)]$, respectively, indicating

$$r\cos^2\theta_1 + r\sin^2\theta_1 + c_1 = 0$$
$$r\cos^2\theta_2 + r\sin^2\theta_2 + c_2 = 0$$

Therefore, we have $c_1 = c_2 = -r$ from which the equations of S_1 and S_2 follow. The proof for the case when O is anticlockwise is also along the same lines. This completes the proof. □

Remark 4. It should be noted that all the proposed properties of the optimal path in Section 4 are obtained only from the necessary conditions at the junction points at time t_i, $i \in \{1, 2\}$. These conditions are independent of the initial and final configuration, which can be any manifold in $\mathbb{R}^2 \times \mathbb{S}^1$.

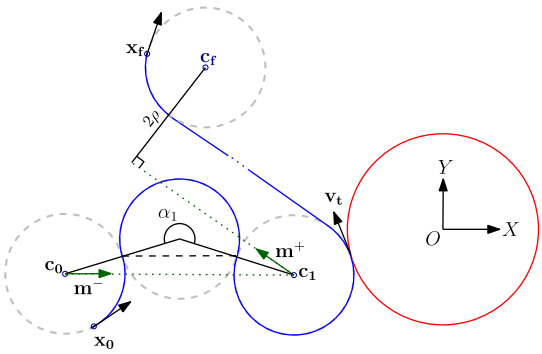

Fig. 4. Geometry of a *LRLSR* path.

5. Analytical solution

Based on the characteristics of optimal path presented in previous section, we are now able to present the analytical solutions by finding the roots of certain polynomials.

5.1. Solution of optimal path with one tangent point

In all categories of path with one tangent point, it is possible to define a unit vector parallel to $\mathbf{m}^-$ and another unit vector parallel to $\mathbf{m}^+$, described in Theorem 4.3 as a function of given initial and final configurations. After this a univariate polynomial is constructed using the results from Theorem 4.3 and the roots of the polynomial give us the candidate heading angles at the tangent point of the optimal path and $\mathcal{C}$. As an illustrative example, we take a case of *LRLSR* as shown in Fig. 4. In this case,

$$\mathbf{m}^- = \frac{\mathbf{c_1} - \mathbf{c_0}}{|\mathbf{c_1} - \mathbf{c_0}|}, \quad \mathbf{m}^+ = \mathrm{R}(\gamma)\frac{\mathbf{c_f} - \mathbf{c_1}}{|\mathbf{c_f} - \mathbf{c_1}|}$$

where $\mathrm{R}(\gamma)$ is the standard two dimensional rotation matrix with $\gamma = \arcsin\left(\frac{2\rho}{|\mathbf{c_f} - \mathbf{c_1}|}\right)$ and $\mathbf{c_i} \in \mathbb{R}^2$, $i \in [0, 1, f]$ are the centers of respective circles shown in Fig. 4. The vectors are given as,

$$\mathbf{c_0} = \begin{bmatrix} x_0 - \rho\sin(\theta_0) \\ y_0 + \rho\cos(\theta_0) \end{bmatrix}, \quad \mathbf{c_1} = \begin{bmatrix} -(r+\rho)\sin(\theta_1) \\ (r+\rho)\cos(\theta_1) \end{bmatrix}$$
$$\mathbf{c_f} = \begin{bmatrix} x_f + \rho\sin(\theta_f) \\ y_f - \rho\cos(\theta_f) \end{bmatrix}$$

and $\cos(\alpha_1) = \frac{8\rho^2 - |\mathbf{c_1} - \mathbf{c_0}|^2}{8\rho^2}$. Using Theorem 4.3 and substituting $\cos(\theta_1) = \frac{1-\tan^2\left(\frac{\theta_1}{2}\right)}{1+\tan^2\left(\frac{\theta_1}{2}\right)}$ and $\sin(\theta_1) = \frac{2\tan\left(\frac{\theta_1}{2}\right)}{1+\tan^2\left(\frac{\theta_1}{2}\right)}$, we obtain the following univariate polynomial with non-negative exponents,

$$\sum_{i=0}^{20} \mathcal{P}_i(\cdot)\tan^i\left(\frac{\theta_1}{2}\right) = 0$$

where $\mathcal{P}_i(\cdot)$ is in terms of $\mathbf{x_0}$, $\mathbf{x_f}$, r and ρ. The high degree of this polynomial occurs due to a change of variable done to avoid non-integral exponents of $\tan\left(\frac{\theta_1}{2}\right)$. Therefore, only real roots of this polynomial that satisfies Eq. (17) along with Theorem 4.2 give candidate optimal values of θ_1.

Similarly, univariate polynomials for other types of paths with one tangent point can be obtained. Table 1 summarizes the degree of polynomial obtained for all path types.

5.2. Solution of optimal path with a nonzero interval overlapping $\mathcal{C}$

Now, the analytical solution of optimal path with segment O will be presented. In Fig. 5, let the heading angle at point $\mathbf{P_i} \in \mathbb{R}^2$

Table 1
Degree of polynomial for each path type.

Degree	Path type
20	*RLRSL*, *LRLSR*, *RSLRL*, *LSRLR*, *LSRSL*, *RSLSR*
16	*RSRSL*, *RSLSL*, *LSRSR*, *LSLSR*
10	*LRLRL*, *RLRLR*
8	*LSLRL*, *LRLSR*, *RSRLR*, *RLRSR*
6	*RSRSR*, *LSLSL*

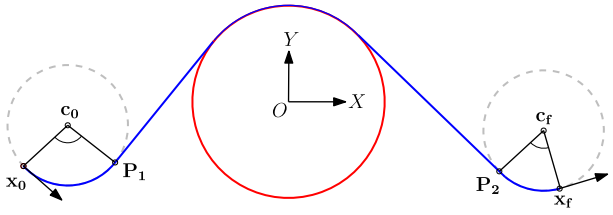

Fig. 5. Geometry of a *CSOSC* path.

be θ_i, $i \in \{1, 2\}$. Then we have,

$$\mathbf{P_1} = \begin{bmatrix} x_0 - l_0\rho\sin\theta_0 + l_0\rho\sin\theta_1 \\ y_0 + l_0\rho\cos\theta_0 - l_0\rho\cos\theta_1 \end{bmatrix}$$

$$\mathbf{P_2} = \begin{bmatrix} x_f - l_f\rho\sin\theta_f + l_f\rho\sin\theta_2 \\ y_f + l_f\rho\cos\theta_f - l_f\rho\cos\theta_2 \end{bmatrix}$$

where $l_i = 1$, for $i \in \{0, f\}$, if the turn at t_i is a left turn (L) and $l_i = -1$ if it is a right turn (R). $\mathbf{P_1}$ and $\mathbf{P_2}$ pass through S_1 and S_2 and therefore from Theorem 4.5, we have

$$(y_0 + l_0\rho\cos\theta_0)\cos\theta_1 - (x_0 - l_0\rho\sin\theta_0)\sin\theta_1 - l_0\rho + \delta r = 0$$
$$\left(y_f + l_f\rho\cos\theta_f\right)\cos\theta_2 - \left(x_f - l_f\rho\sin\theta_f\right)\sin\theta_2 - l_f\rho + \delta r = 0$$

From the above two equations, the expressions of θ_1 and θ_2 can be obtained as,

$$\theta_{\{1,2\}} = \arccos\left(\frac{\left(l_{\{0,f\}}\rho - \delta r\right)\left(l_{\{0,f\}}\rho\cos\theta_{\{0,f\}} + y_{\{0,f\}}\right)}{\mu + \rho^2}\right.$$
$$\left.\pm\frac{\left(x_{\{0,f\}} - l_{\{0,f\}}\rho\sin\theta_{\{0,f\}}\right)\sqrt{\mu - r^2 + 2l_{\{0,f\}}\delta\rho r}}{\mu + \rho^2}\right)$$

where $\mu = 2l_{\{0,f\}}\rho\left(y_{\{0,f\}}\cos(\theta_{\{0,f\}}) - x_{\{0,f\}}\sin(\theta_{\{0,f\}})\right) + x_{\{0,f\}}^2 + y_{\{0,f\}}^2$.

6. Numerical simulations

Some numerical examples are presented in this section to demonstrate the developments of the paper. The optimal paths are calculated by finding the roots of the univariate polynomials obtained from Theorems 4.3 and 4.5. The roots of the polynomial can be calculated efficiently by calculating the eigenvalues of its companion matrix (Rowland, 2020) as shown in Chen and Shima (2019). On a system with Intel(R) Core(TM) i7-4790 CPU @3.60 GHz and 16.0 GB RAM , a large number of examples (generated randomly) are simulated, showing that the optimal path can be calculated within 930.4 μs. In a special case when the initial and final configurations are at a distance of at least 4ρ from the intermediate circle, then the possibility of *CCCCC*, *CSCCC* and *CCCSC* paths is ruled out and hence the computation time did not exceed 441.8 μs.

6.1. Numerical examples

Fig. 6 shows a case selected from simulations for which the optimal path has one tangent point on the circle $\mathcal{C}$. Here, $r = 4$, $\rho = 6$, $\mathbf{x_0} = \left[-20, -15, -\frac{\pi}{4}\right]^\top$, and $\mathbf{x_f} = \left[10, -15, \frac{\pi}{2}\right]^\top$. In this case we obtain a *LSRSR* path that verifies the results from Theorem 4.2 and Corollary 2. It can be seen that the arc lengths of the circular segments before and after the tangent point $(0.85, -3.90)$ are equal and the turn directions of the both the circular segments are the same.

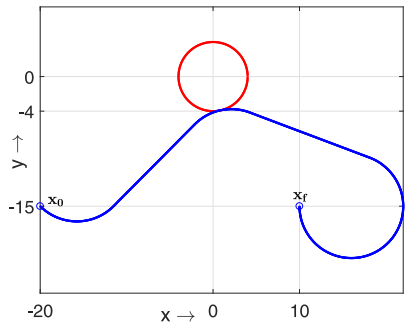

Fig. 6. Optimal path with only one tangent point ($\rho > r$).

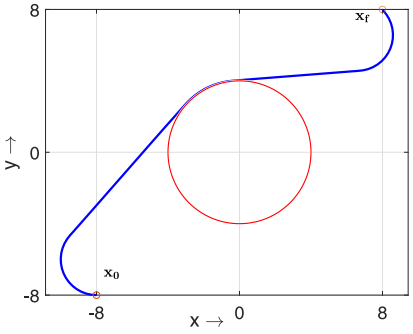

Fig. 7. Optimal path with O-segment.

Fig. 7 shows a case selected from the simulations for which the optimal path is with a segment O. Here, $\rho = 2$, $r = 4$, and the initial and final conditions are $\mathbf{x_0} = [-8, -8, -\pi]^\top$ and $\mathbf{x_f} = \left[6, 8, \frac{3\pi}{4}\right]^\top$, respectively. It can be seen that an O-segment is preceded and succeeded by a S-segment as proved in Lemma 4.4.

6.2. Dubins traveling salesman problem with neighborhoods

The descent method in Chen et al. (2020) and Váňa and Faigl (2015) for the DTSPN requires the solution of a subproblem which is of finding the shortest Dubins path from a configuration, via a circular region, to another configuration. For this subproblem, the solution path is readily available if the shortest Dubins path from initial configuration to the final configuration intersects the intermediate circle. If it does not intersect the intermediate circle, this subproblem is equivalent to what has been solved in the present paper. Thus, the developments of the paper can be applied to address the DTSPN.

In this subsection, two DTSPNs will be addressed by the descent method to demonstrate the developments of the paper. In both the cases, the sequence of the target region is ordered in advance by the solution from Euclidean Traveling Salesman Problem (ETSP). Then, by embedding the developments of the paper into the descent method proposed in Chen et al. (2020) and Váňa and Faigl (2015), the DTSPN solution is obtained.

We first consider a case of DTSPN with 30 randomly generated circular regions of radius $r = 6$ and turn radius $\rho = 3$ as presented in Fig. 8. We can see that every target region in Fig. 8 is visited and all the paths generated for each subproblem are of type *CSCSC*. The second case of DTSPN consists of 10 circular

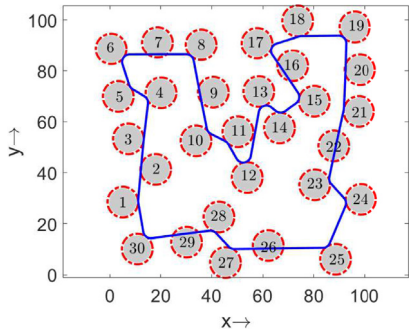

Fig. 8. DTSPN with 30 targets, $r = 6$, $\rho = 3$.

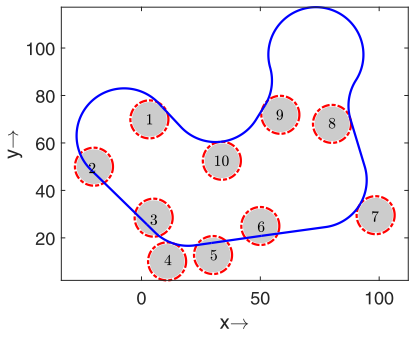

Fig. 9. DTSPN with 10 targets, $r = 8$, $\rho = 20$.

regions with radius of $r = 8$ and $\rho = 20$. Here, the assumption about minimum separation distance of 4ρ of the initial and final configuration from the intermediate circle (Chen et al., 2020; Váňa & Faigl, 2015) does not hold. Thanks to the developments of our paper where no assumption on separation distances between the targets is considered, the second case of DTSPN can also be addressed by applying the descent algorithm. The solution is presented in Fig. 9. We can see from Fig. 9 that the solution not only includes CSCSC paths but also includes CSCCC paths.

7. Conclusions

The properties of the shortest bounded-curvature path between two configurations via the boundary of an intermediate circle were established using Pontryagin's maximum principle and necessary conditions for state inequality constraints. It was shown that the optimal paths are sequence of only straight line segments (S) and two types of circular segments (C and O). These properties give us insights about how these segments are concatenated and thereby restrict the number of candidate paths to a finite set of 26 types. In the case when the optimal path has only one tangent point to the intermediate circle, the turn directions of the circular segments prior and subsequent to the tangent point are equal. In addition to it, the center of the intermediate circle, the tangent point, and the intersection point of two lines joining all points of concatenations before and after the tangent point, respectively, are collinear. For the case when a segment of the optimal path overlaps the circular boundary, the segment before and after the overlapping segment must be a straight line segment. These properties were further used to devise analytical solutions for all possible candidate paths. Numerical examples justifying the established geometric properties were presented. The applicability of the proposed theorems to the case of DTSPN was also presented.

References

Bellman, Richard (1966). Dynamic programming. *Science*, *153*(3731), 34–37.

Boissonnat, Jean-Daniel, Cérézo, André, & Leblond, Juliette (1994). Shortest paths of bounded curvature in the plane. *Journal of Intelligent and Robotic Systems*, *11*(1–2), 5–20.

Bryson, Arthur E., Denham, Walter F., & Dreyfus, Stewart E. (1963). Optimal programming problems with inequality constraints. *AIAA Journal*, *1*(11), 2544–2550.

Bui, Xuân-Nam, Boissonnat, J-D, Soueres, Philippe, & Laumond, J-P (1994). Shortest path synthesis for Dubins non-holonomic robot. In *Proceedings of the 1994 IEEE international conference on robotics and automation* (pp. 2–7). IEEE.

Chen, Zheng (2020). On Dubins paths to a circle. *Automatica*, *117*, Article 108996.

Chen, Zheng, & Shima, Tal (2019). Shortest Dubins paths through three points. *Automatica*, *105*, 368–375.

Chen, Zheng, Sun, Chenhao, Shao, Xueming, & Zhao, Wenjie (2020). A descent method for Dubins traveling salesman problem with neighborhoods. *Frontiers of Information Technology and Electronic Engineering* http://dx.doi.org/10.1631/FITEE.2000041.

Dubins, Lester E. (1957). On curves of minimal length with a constraint on average curvature, and with prescribed initial and terminal positions and tangents. *American Journal of Mathematics*, *79*(3), 497–516.

Gerdts, Matthias (2011). *Optimal control of ODEs and DAEs*. Walter de Gruyter.

Girsanov, Igor Vladimirovich (2012). *Lectures on mathematical theory of extremum problems (vol. 67)*. Springer Science and Business Media.

Goaoc, Xavier, Kim, Hyo-Sil, & Lazard, Sylvain (2013). Bounded-curvature shortest paths through a sequence of points using convex optimization. *SIAM Journal on Computing*, *42*(2), 662–684.

Guimaraes Macharet, Douglas, Alves Neto, Armando, Fiuza da Camara Neto, Vilar, & Montenegro Campos, Mario (2012). An evolutionary approach for the dubins' traveling salesman problem with neighborhoods. In *Proceedings of the 14th annual conference on genetic and evolutionary computation* (pp. 377–384).

Hartl, Richard F., Sethi, Suresh P., & Vickson, Raymond G. (1995). A survey of the maximum principles for optimal control problems with state constraints. *SIAM Review*, *37*(2), 181–218.

Ioffe, Aleksandr Davidovich, & Tihomirov, Vladimir Mihajlovič (2009). *Theory of extremal problems*. Elsevier.

Isaacs, Jason, & Hespanha, João (2013). Dubins traveling salesman problem with neighborhoods: A graph-based approach. *Algorithms*, *6*(1), 84–99.

Isaacs, Jason T., Klein, Daniel J., & Hespanha, Joao P. (2011). Algorithms for the traveling salesman problem with neighborhoods involving a dubins vehicle. In *Proceedings of the 2011 American control conference* (pp. 1704–1709). IEEE.

Isaiah, Pantelis, & Shima, Tal (2015). Motion planning algorithms for the Dubins travelling salesperson problem. *Automatica*, *53*, 247–255.

Jacobson, David H., Lele, Milind M., & Speyer, Jason L. (1971). New necessary conditions of optimality for control problems with state-variable inequality constraints. *Journal of Mathematical Analysis and Applications*, *35*(2), 255–284.

Jha, Bhargav, Chen, Zheng, & Shima, Tal (2020). Shortest bounded-curvature paths via circumferential envelope of a circle. *IFAC Proceedings Volumes*.

Jha, Bhargav, Tsalik, Ronny, Weiss, Martin, & Shima, Tal (2019). Cooperative guidance and collision avoidance for multiple pursuers. *Journal of Guidance, Control, and Dynamics*, *42*(7), 1506–1518.

Johnson, Harold H. (1974). An application of the maximum principle to the geometry of plane curves. *Proceedings of the Americal Mathematical Society*, *44*(2), 432–435.

Kreindler, E. (1982). Additional necessary conditions for optimal control with state-variable inequality constraints. *Journal of Optimization Theory and Applications*, *38*(2), 241–250.

LaValle, Steven M. (2006). *Planning algorithms*. Cambridge University Press.

Liberzon, Daniel (2011). *Calculus of variations and optimal control theory: A concise introduction*. Princeton University Press.

Manor, Gil, Ben-Asher, Joseph Z., & Rimon, Elon (2018). Time optimal trajectories for a mobile robot under explicit acceleration constraints. *IEEE Transactions on Aerospace and Electronic Systems*, *54*(5), 2220–2232.

Markov, Andrey Andreyevich (1887). Some examples of the solution of a special kind of problem on greatest and least quantities. *Soobshch. Karkovsk. Mat. Obshch (in Russian)*, *1*, 250–276.

Matveev, Alexey S., Magerkin, Valentin V., & Savkin, Andrey V. (2020). A method of reactive control for 3D navigation of a nonholonomic robot in tunnel-like environments. *Automatica*, *114*, Article 108831.

Mylvaganam, Thulasi, Sassano, Mario, & Astolfi, Alessandro (2017). A differential game approach to multi-agent collision avoidance. *IEEE Transactions on Automatic Control*, *62*(8), 4229–4235.

Noon, Charles E., & Bean, James C. (1993). An efficient transformation of the generalized traveling salesman problem. *INFOR: Information Systems and Operational Research*, *31*(1), 39–44.

Ny, Jerome, Feron, Eric, & Frazzoli, Emilio (2011). On the Dubins traveling salesman problem. *IEEE Transactions on Automatic Control*, *57*(1), 265–270.

Obermeyer, Karl (2009). Path planning for a UAV performing reconnaissance of static ground targets in terrain. In *AIAA guidance, navigation, and control conference* (p. 5888).

Obermeyer, Karl J., Oberlin, Paul, & Darbha, Swaroop (2012). Sampling-based path planning for a visual reconnaissance unmanned air vehicle. *Journal of Guidance, Control, and Dynamics*, *35*(2), 619–631.

Pontryagin, Lev Semenovich (2018). *Mathematical theory of optimal processes*. Routledge.

Reeds, James, & Shepp, Lawrence (1990). Optimal paths for a car that goes both forwards and backwards. *Pacific Journal of Mathematics*, *145*(2), 367–393.

Rowland, Todd (2020). Companian matrix. From MathWorld–a wolfram web resource. (Accessed 14 May 2020).

Salaris, Paolo, Cristofaro, Andrea, Pallottino, Lucia, & Bicchi, Antonio (2014). Epsilon-optimal synthesis for vehicles with vertically bounded field-of-view. *IEEE Transactions on Automatic Control*, *60*(5), 1204–1218.

Savkin, Andrey V., & Hoy, Michael (2013). Reactive and the shortest path navigation of a wheeled mobile robot in cluttered environments. *Robotica*, *31*(2), 323–330.

Sunkara, V., Chakravarthy, A., & Ghose, D. (2019). Collision avoidance of arbitrarily shaped deforming objects using collision cones. *IEEE Robotics and Automation Letters*, *4*(2), 2156–2163.

Sussmann, Héctor J., & Tang, Guoqing (1991). *Shortest paths for the Reeds-Shepp car: A worked out example of the use of geometric techniques in nonlinear optimal control*: *Rutgers center for systems and control technical report, 10*, (pp. 1–71).

Tripathy, Twinkle, & Sinha, Arpita (2017). Unicycle with only range input: An array of patterns. *IEEE Transactions on Automatic Control*, *63*(5), 1300–1312.

Tsourdos, Antonios, White, Brian, & Shanmugavel, Madhavan (2010). *Cooperative path planning of unmanned aerial vehicles (vol. 32)*. John Wiley & Sons.

Váňa, Petr, & Faigl, Jan (2015). On the dubins traveling salesman problem with neighborhoods. In *2015 IEEE/RSJ international conference on intelligent robots and systems* (pp. 4029–4034). IEEE.

Wright, Stephen J. (2015). Coordinate descent algorithms. *Mathematical Programming*, *151*(1), 3–34.

Bhargav Jha received his B.E. (Hons) degree in Electronics and Instrumentation Engineering from Birla Institute of Technology & Science Pilani, India in 2016 and the Master Degree in Aerospace Engineering from Technion-Israel Institute of Technology in 2019. He is currently pursuing his Ph.D. degree from the Faculty of Aerospace Engineering at Technion. His current research interests include motion planning, optimal control, and development of cooperative guidance and control strategies for autonomous vehicles with a particular emphasis on their practical implementation.

Zheng Chen received the Ph.D. degree in Applied Mathematics from the University Paris-Saclay in 2016, the M.Sc and B.Sc in Aerospace Engineering from Northwestern Polytechnical University in 2013 and 2010, respectively. He is currently a professor with the School of Aeronautics and Astronautics at Zhejiang University. His current research interests revolve around guidance and control in aerospace engineering.

Tal Shima received his B.Sc., MA, and Ph.D. degrees, all in Aerospace Engineering, from the Technion - Israel Institute of Technology, in 1992, 1998, and 2001, respectively. He also received the MBA degree from the Tel-Aviv University in 1997.

From 2000 to 2004 he was with the Air-to-Air and Surface-to-Air Directorate of RAFAEL Ltd.. In 2004 and 2005 he was awarded National Research Council scholarships for performing research at the US Air Force Research Labs, WrightPatterson AFB, OH. Since 2006 Dr. Shima is with the Department of Aerospace Engineering at the Technion, where he is currently a Full Professor and Dean.

His current research interests are in the area of guidance of autonomous vehicles, especially missiles and aircraft, operating individually or as a team. Specific interests are: 1-on-1 guidance; Cooperative guidance; and Guidance integrated with task assignment, autopilot, and estimation. He is the author/coauthor of more than 90 archival journal papers in these research areas.